

Insights in quantum dynamical effects in the infrared spectroscopy of liquid water from a semiclassical study with an ab initio-based flexible and polarizable force field

Jian Liu, William H. Miller, George S. Fanourgakis, Sotiris S. Xantheas, Sho Imoto, and Shinji Saito

Citation: *J. Chem. Phys.* **135**, 244503 (2011); doi: 10.1063/1.3670960

View online: <https://doi.org/10.1063/1.3670960>

View Table of Contents: <http://aip.scitation.org/toc/jcp/135/24>

Published by the [American Institute of Physics](#)

Articles you may be interested in

[Quantum dynamical effects in liquid water: A semiclassical study on the diffusion and the infrared absorption spectrum](#)

The Journal of Chemical Physics **131**, 164509 (2009); 10.1063/1.3254372

[Path integral Liouville dynamics for thermal equilibrium systems](#)

The Journal of Chemical Physics **140**, 224107 (2014); 10.1063/1.4881518

[An approach for generating trajectory-based dynamics which conserves the canonical distribution in the phase space formulation of quantum mechanics. I. Theories](#)

The Journal of Chemical Physics **134**, 104101 (2011); 10.1063/1.3555273

[Path integral Liouville dynamics: Applications to infrared spectra of OH, water, ammonia, and methane](#)

The Journal of Chemical Physics **144**, 034307 (2016); 10.1063/1.4939953

[A simple and accurate algorithm for path integral molecular dynamics with the Langevin thermostat](#)

The Journal of Chemical Physics **145**, 024103 (2016); 10.1063/1.4954990

[A unified thermostat scheme for efficient configurational sampling for classical/quantum canonical ensembles via molecular dynamics](#)

The Journal of Chemical Physics **147**, 034109 (2017); 10.1063/1.4991621

PHYSICS TODAY

WHITEPAPERS

ADVANCED LIGHT CURE ADHESIVES

Take a closer look at what these environmentally friendly adhesive systems can do

READ NOW

PRESENTED BY
 MASTERBOND
ADHESIVES | SEALANTS | COATINGS

Insights in quantum dynamical effects in the infrared spectroscopy of liquid water from a semiclassical study with an *ab initio*-based flexible and polarizable force field

Jian Liu,¹ William H. Miller,^{1,a)} George S. Fanourgakis,² Sotiris S. Xantheas,³ Sho Imoto,⁴ and Shinji Saito^{4,5}

¹Department of Chemistry and K. S. Pitzer Center for Theoretical Chemistry, University of California, and Chemical Science Division, Lawrence Berkeley National Laboratory, Berkeley, California 94720-1460, USA

²Institute of Electronic Structure and Laser, Foundation for Research and Technology-Hellas, GR-711 10, Heraklion, Greece

³Chemical and Materials Sciences Division, Pacific Northwest National Laboratory, 902 Battelle Boulevard, P.O. Box 999, MS K1-83, Richland, Washington 99352, USA

⁴Graduate University for Advanced Studies, Myodaiji, Okazaki, Aichi 444-8585, Japan

⁵Department of Theoretical and Computational Molecular Science, Institute for Molecular Science, Myodaiji, Okazaki, Aichi 444-8585, Japan

(Received 31 August 2011; accepted 30 November 2011; published online 28 December 2011)

The dynamical properties of liquid water play an important role in many processes in nature. In this paper, we focus on the infrared (IR) absorption spectrum of liquid water based on the linearized semiclassical initial value representation (LSC-IVR) with the local Gaussian approximation (LGA) [J. Liu and W. H. Miller, *J. Chem. Phys.* **131**, 074113 (2009)] and an *ab initio* based, flexible, polarizable Thole-type model (TTM3-F) [G. S. Fanourgakis and S. S. Xantheas, *J. Chem. Phys.* **128**, 074506 (2008)]. Although the LSC-IVR (LGA) gives the exact result for the isolated three-dimensional shifted harmonic stretching model, it yields a blueshifted peak position for the more realistic anharmonic stretching potential. By using the short-time information of the LSC-IVR correlation function; however, it is shown how one can obtain more accurate results for the position of the stretching peak. Due to the physical decay in the condensed phase system, the LSC-IVR (LGA) is a good and practical approximate quantum approach for the IR spectrum of liquid water. The present results offer valuable insight into future attempts to improve the accuracy of the TTM3-F potential or other *ab initio*-based models in reproducing the IR spectrum of liquid water. © 2011 American Institute of Physics. [doi:10.1063/1.3670960]

I. INTRODUCTION

Real-time quantum dynamics simulations of large molecular systems present a challenge to theoretical physics and chemistry. The most accurate treatment is of course a complete solution of the time-dependent Schrödinger equation or of the real-time path integral (which is impractical to apply for large systems), while classical molecular dynamics (MD) fails to capture quantum effects. Semiclassical (SC) theory^{1,2} stands between these two limits: it utilizes classical trajectories as “input,” and thus contains classical dynamics, and incorporates quantum mechanics approximately, i.e., within the SC approximation. The SC approximation actually contains *all* quantum effects at least qualitatively, and in molecular systems the description is usually quite quantitative. Various initial value representations (IVRs) of SC theory (primarily to calculate time correlation functions^{3,4}) can provide practical tools for including quantum effects in large systems.

The simplest (and most approximate) version of the SC-IVR is its “linearized” approximation (LSC-IVR).⁵⁻⁷ The LSC-IVR cannot describe true quantum coherence effects in time correlation functions—more accurate SC-IVR

approaches⁴ are needed for this—but it does describe a number of aspects of the dynamics very well.⁷⁻²¹ For instance, the LSC-IVR has been shown to describe reactive flux correlation functions for chemical reaction rates quite well, including strong tunneling regimes,^{5,7,22} and correlation functions¹⁰⁻²¹ in systems with enough degrees of freedom for quantum rephasing to be unimportant. More recently, Liu and Miller have proposed a local Gaussian approximation (LGA) for treating imaginary frequencies⁷ with the LSC-IVR, which provides a practical tool to study quantum effects in large/complex molecular systems whose interactions are often too difficult to be parameterized by Gaussians or polynomials and where *ab initio* dynamics is called for.

The LSC-IVR/classical Wigner model gives the exact quantum correlation function in the short time^{5,23} ($t \rightarrow 0$), classical ($\hbar \rightarrow 0$), and high-temperature ($\beta \rightarrow 0$) limits and for harmonic potentials^{16,24-27} (even for nonlinear operators, i.e., nonlinear functions of the position or momentum operators). The LSC-IVR has the drawback that the distribution generated for the operator \hat{A}^β is not invariant with time for the case $\hat{A} = 1$ (that is, $\hat{A}^\beta = e^{-\beta\hat{H}}$, the Boltzmann operator itself) for anharmonic systems, which can be a serious problem if the long-time behavior of the correlation function is important.^{13,24-30} The failure to conserve the quantum

^{a)} Author to whom correspondence should be addressed. Electronic mail: millerwh@berkeley.edu.

canonical distribution very likely makes a significant contribution to the unphysical decay (i.e., overdamping) intrinsic in the LSC-IVR correlation function, which becomes progressively worse for longer times.^{13,24–27,30,31} As a part of the effects due to the failure of the LSC-IVR to conserve the quantum canonical distribution, the artificial energy flow exists from intramolecular to intermolecular modes for such a system as liquid water, as observed by Poulsen and Rossky [e.g., see the note (Ref. 36) of Ref. 32] and by Liu and Miller.¹⁵ Haberson and Manolopoulos further studied the artificial flow (in more detail) and linked it with another notation—so-called zero-point energy leakage,³⁰ which they argued that could be the main source of error for quantities that involve long-time behaviors for liquid water. (Also see Appendix A.)

Since the infrared (IR) spectrum of the large molecular system is often connected to ultrafast dynamics [i.e., the physical time scale of the dipole-derivative correlation function (whose Fourier transform at finite frequencies leads to the IR spectrum) is relatively short—about several hundred femtoseconds], the intrinsic unphysical decay of the LSC-IVR correlation function, as discussed above, will be greatly compensated by the inherent physical decay in the system. We note this is actually the main reason why the LSC-IVR is a good approximate quantum approach for study of the IR spectrum.^{15,30} The purpose of this paper is to present a further systematic investigation as an extension of our earlier work.¹⁵ We focus on the IR absorption spectrum. Section II first briefly reviews the LSC-IVR (LGA) methodology for time correlation functions, and Sec. III then gives the explicit formulation for the dipole-derivative correlation function for the IR spectrum (for which the dipole or dipole-derivative operator can be a nonlinear operator). Section IV tests the LSC-IVR for the vibrational IR spectrum of the isolated OH molecule and then studies the IR spectrum of liquid water with the *ab initio* based flexible, polarizable TTM3-F model³³ at the ambient condition (300 K), followed by further discussions. Section V summarizes and concludes.

II. SIMULATION METHODOLOGY

A. Linearized semiclassical initial value representation for the correlation function

Most dynamical properties can be expressed in terms of thermal time correlation functions,³⁴ which are of the form

$$C_{AB}(t) = \frac{1}{Z} \text{Tr}(\hat{A}^\beta e^{i\hat{H}t/\hbar} \hat{B} e^{-i\hat{H}t/\hbar}), \quad (1)$$

where $\hat{A}_{std}^\beta = e^{-\beta\hat{H}} \hat{A}$ for the standard version of the correlation function, or $\hat{A}_{sym}^\beta = e^{-\beta\hat{H}/2} \hat{A} e^{-\beta\hat{H}/2}$ for the symmetrized version,³⁵ or $\hat{A}_{Kubo}^\beta = \frac{1}{\beta} \int_0^\beta d\lambda e^{-(\beta-\lambda)\hat{H}} \hat{A} e^{-\lambda\hat{H}}$ for the Kubo-transformed version.³⁶ These three versions are related to one another by the following identities between their Fourier transforms:

$$\frac{\beta\hbar\omega}{1 - e^{-\beta\hbar\omega}} I_{AB}^{Kubo}(\omega) = I_{AB}^{std}(\omega) = e^{\beta\hbar\omega/2} I_{AB}^{sym}(\omega), \quad (2)$$

where $I_{AB}(\omega) = \int_{-\infty}^{\infty} dt e^{-i\omega t} C_{AB}(t)$, etc. Here, $Z = \text{Tr}[e^{-\beta\hat{H}}]$ ($\beta = 1/k_B T$) is the partition function

and \hat{H} is the (time-independent) Hamiltonian of the system, and \hat{A} and \hat{B} are operators relevant to the specific property of interest.

The SC-IVR approximates the forward (backward) time evolution operator $e^{-i\hat{H}t/\hbar}$ ($e^{i\hat{H}t/\hbar}$) by a phase space average over the initial conditions of forward (backward) classical trajectories.^{1,3,4,37} By making the approximation that the dominant contribution to the phase space averages comes from forward and backward trajectories that are infinitesimally close to one another, and then linearizing the difference between the forward and backward actions (and other quantities in the integrand), Miller and co-workers^{5,8} (see also Ref. 38) obtained the LSC-IVR, or classical Wigner model for the correlation function in Eq. (1),

$$C_{AB}^{LSC-IVR}(t) = Z^{-1} (2\pi\hbar)^{-3N} \int d\mathbf{x}_0 \times \int d\mathbf{p}_0 A_w^\beta(\mathbf{x}_0, \mathbf{p}_0) B_w(\mathbf{x}_t, \mathbf{p}_t), \quad (3)$$

where A_w^β and B_w are the Wigner functions^{39,40} corresponding to these operators

$$O_w(\mathbf{x}, \mathbf{p}) = \int d\Delta\mathbf{x} \langle \mathbf{x} - \Delta\mathbf{x}/2 | \hat{O} | \mathbf{x} + \Delta\mathbf{x}/2 \rangle e^{i\mathbf{p}^T \Delta\mathbf{x}/\hbar} \quad (4)$$

for any operator \hat{O} . Here, N is the number of particles in the system, and $(\mathbf{x}_0, \mathbf{p}_0)$ is the set of initial conditions (i.e., coordinates and momenta) for a classical trajectory, $(\mathbf{x}_t(\mathbf{x}_0, \mathbf{p}_0), \mathbf{p}_t(\mathbf{x}_0, \mathbf{p}_0))$ being the phase point at time t along this trajectory.

The classical Wigner model is an old idea,^{39,41–43} but it is informative to realize that it is contained within the general SC-IVR formulation, namely, as a specific approximation to it;^{5,8} more accurate implementations of the SC-IVR approach would be expected to lead to a more accurate description. It should also be noted that there are other approximate routes^{6,21,24,26,44} which lead to the classical Wigner model for correlation functions (other than simply postulating it). Moreover, Liu and Miller^{24,26} have recently shown that the exact quantum time correlation function can be expressed in the same form as Eq. (3), with an associated dynamics in the single phase space, and it was furthermore demonstrated that the LSC-IVR is its classical limit ($\hbar \rightarrow 0$), high temperature limit ($\beta \rightarrow 0$), and harmonic limit (even for correlation functions involving nonlinear operators). Note all these approximate routes also indicate that the LSC-IVR is the short-time approximation ($t \rightarrow 0$) to the quantum correlation function. This has been well demonstrated by the maximum entropy analytical continuation test for condensed phase systems.¹⁴

B. Local Gaussian approximation

Calculation of the Wigner function for operator \hat{B} in Eq. (3) is usually straightforward; in fact, \hat{B} is often a function only of coordinates or only of momenta, in which case its Wigner function is simply the classical function itself. Calculating the Wigner function for operator \hat{A}^β , however, involves the Boltzmann operator with the total Hamiltonian of the complete system, so that carrying out the multidimensional Fourier transform to obtain it is non-trivial. Furthermore, it is

necessary to do this in order to obtain the distribution of initial conditions of momenta \mathbf{p}_0 for the real-time trajectories. To accomplish this task, several approximations^{5,11,16,21} have been introduced for the LSC-IVR. More recently, Liu and Miller have proposed a LGA that improves on all these approximations for treating imaginary frequencies,⁷ and this is what we have used for the study of liquid water in this paper. Below we briefly summarize the version of LGA developed based on the local harmonic approximation of Shi and Geva.¹⁶

As in the standard normal-mode analysis, mass-weighted Hessian matrix elements are given by

$$H_{kl} = \frac{1}{\sqrt{m_k m_l}} \frac{\partial^2 V}{\partial x_k \partial x_l}, \quad (5)$$

where m_k represent the mass of the k th degree of freedom with $3N$ the total number of degrees of freedom. The Hamiltonian around \mathbf{x} can be expanded to 2nd order as

$$H(\mathbf{x} + \Delta\mathbf{x}) \approx \frac{1}{2} \mathbf{p}^T \mathbf{M}^{-1} \mathbf{p} + V(\mathbf{x}) + \left(\frac{\partial V}{\partial \mathbf{x}} \right)^T \Delta\mathbf{x} + \frac{1}{2} \Delta\mathbf{x}^T H \Delta\mathbf{x}. \quad (6)$$

The eigenvalues of the mass-weighted Hessian matrix produce normal-mode frequencies $\{\omega_k\}$, i.e.,

$$\mathbf{T}^T H \mathbf{T} = \lambda \quad (7)$$

with λ a diagonal matrix with the elements $\{(\omega_k)^2\}$ and \mathbf{T} an orthogonal matrix. If \mathbf{M} is the diagonal “mass matrix” with elements $\{m_k\}$, then the mass-weighted normal mode coordinates and momenta (\mathbf{X}, \mathbf{P}) are given in terms of the Cartesian variables (\mathbf{x}, \mathbf{p}) by

$$\mathbf{X} = \mathbf{T}^T \mathbf{M}^{1/2} \mathbf{x}, \quad (8)$$

$$\mathbf{P} = \mathbf{T}^T \mathbf{M}^{-1/2} \mathbf{p}, \quad (9)$$

and

$$\Delta\mathbf{X} = \mathbf{T}^T \mathbf{M}^{1/2} \Delta\mathbf{x}. \quad (10)$$

Equation (6) can be expressed as

$$H(\mathbf{x} + \Delta\mathbf{x}) \equiv H(\mathbf{X} + \Delta\mathbf{X}) \approx \frac{1}{2} \mathbf{P}^T \mathbf{P} + V(\mathbf{X}) + \Delta\mathbf{X}^T \mathbf{F} + \frac{1}{2} \Delta\mathbf{X}^T \lambda \Delta\mathbf{X} \quad (11)$$

with \mathbf{F} as the force in the mass-weighted normal mode coordinates

$$\mathbf{F} = \mathbf{T}^T \mathbf{M}^{-1/2} \left(\frac{\partial V}{\partial \mathbf{x}} \right). \quad (12)$$

By virtue of the fact that

$$\frac{\langle x - \frac{\Delta x}{2} | e^{-\beta \hat{H}} | x + \frac{\Delta x}{2} \rangle}{\langle x | e^{-\beta \hat{H}} | x \rangle} = \exp \left[-\frac{m Q(u)}{2 \hbar^2 \beta} (\Delta x)^2 \right] \quad (13)$$

for the one-dimensional (1d) harmonic case which was implemented in LHA by Shi and Geva,¹⁶ it is straightforward to

show the Wigner function of the Boltzmann operator $e^{-\beta \hat{H}}$ is given by

$$P_W^{eq}(\mathbf{x}, \mathbf{P}) = \langle \mathbf{x} | e^{-\beta \hat{H}} | \mathbf{x} \rangle \prod_{k=1}^{3N} \left[\left(\frac{\beta}{2\pi Q(u_k)} \right)^{1/2} \exp \left[-\beta \frac{(P_k)^2}{2Q(u_k)} \right] \right], \quad (14)$$

where $u_k = \beta \hbar \omega_k$, P_k is the k th component of the mass-weighted normal-mode momentum \mathbf{P} (in Eq. (9)) and the quantum correction factor with the LGA ansatz proposed by Liu and Miller⁷ for both real and imaginary frequencies is given by

$$Q(u) = \begin{cases} \frac{u/2}{\tanh(u/2)} & \text{for real } u \\ \frac{1}{Q(iu)} = \frac{\tanh(iu/2)}{iu/2} & \text{for imaginary } u \ (u = iu_i) \end{cases}. \quad (15)$$

In terms of the phase space variables (\mathbf{x}, \mathbf{p}) , Eq. (14) thus becomes

$$P^{eq, LGA}(\mathbf{x}, \mathbf{p}) = \langle \mathbf{x} | e^{-\beta \hat{H}} | \mathbf{x} \rangle \left(\frac{\beta}{2\pi} \right)^{3N/2} |\det(\mathbf{M}_{therm}^{-1}(\mathbf{x}))|^{1/2} \times \exp \left[-\frac{\beta}{2} \mathbf{p}^T \mathbf{M}_{therm}^{-1} \mathbf{p} \right] \quad (16)$$

with the thermal mass matrix \mathbf{M}_{therm} given by

$$\mathbf{M}_{therm}^{-1}(\mathbf{x}) = \mathbf{M}^{-1/2} \mathbf{T} \mathbf{Q}(\mathbf{u})^{-1} \mathbf{T}^T \mathbf{M}^{-1/2} \quad (17)$$

and the diagonal matrix $\mathbf{Q}(\mathbf{u}) = \{Q(u_k)\}$.

The explicit form of the LSC-IVR correlation function (Eq. (1)) with the LGA is thus given by

$$C_{AB}^{LSC-IVR}(t) = \frac{1}{Z} \int d\mathbf{x}_0 \langle \mathbf{x}_0 | e^{-\beta \hat{H}} | \mathbf{x}_0 \rangle \int d\mathbf{p}_0 \prod_{k=1}^N \left[\left(\frac{\beta}{2\pi Q(u_k)} \right)^{1/2} \exp \left[-\beta \frac{(P_{0,k})^2}{2Q(u_k)} \right] \right] \times f_A(\mathbf{x}_0, \mathbf{p}_0) B(\mathbf{x}_t, \mathbf{p}_t), \quad (18)$$

where

$$f_A(\mathbf{x}_0, \mathbf{p}_0) = \int d\Delta\mathbf{x} \frac{\langle \mathbf{x}_0 - \frac{\Delta\mathbf{x}}{2} | \hat{A}^\beta | \mathbf{x}_0 + \frac{\Delta\mathbf{x}}{2} \rangle}{\langle \mathbf{x}_0 | e^{-\beta \hat{H}} | \mathbf{x}_0 \rangle} e^{i \Delta\mathbf{x}^T \cdot \mathbf{p}_0 / \hbar} \int d\Delta\mathbf{x} \frac{\langle \mathbf{x}_0 - \frac{\Delta\mathbf{x}}{2} | e^{-\beta \hat{H}} | \mathbf{x}_0 + \frac{\Delta\mathbf{x}}{2} \rangle}{\langle \mathbf{x}_0 | e^{-\beta \hat{H}} | \mathbf{x}_0 \rangle} e^{i \Delta\mathbf{x}^T \cdot \mathbf{p}_0 / \hbar} \quad (19)$$

is a function depending on the operator \hat{A}^β . The procedure for implementing the LSC-IVR (LGA) is described in Ref. 7.

III. INFRARED SPECTRUM AND DIPOLE-DERIVATIVE CORRELATION FUNCTION

The experimental IR spectrum is given in terms of two frequency-dependent properties—the Beer-Lambert absorption constant $\alpha(\omega)$ and the refractive index $n(\omega)$. According to

the Fermi Golden Rule of time-dependent perturbation theory in quantum mechanics, these quantities are directly related to the dipole-derivative absorption line shape^{15,45} $I_{\hat{\mu}\hat{\mu}}^{\text{Kubo}}(\omega)$ by

$$n(\omega)\alpha(\omega) = \frac{\beta\pi}{3cV\varepsilon_0} I_{\hat{\mu}\hat{\mu}}^{\text{Kubo}}(\omega), \quad (20)$$

where $I_{\hat{\mu}\hat{\mu}}^{\text{Kubo}}(\omega)$ is the Fourier transform of the (Kubo-transformed) collective dipole-derivative auto-correlation function

$$\begin{aligned} I_{\hat{\mu}\hat{\mu}}^{\text{Kubo}}(\omega) &= \frac{1}{2\pi} \int_{-\infty}^{\infty} dt e^{-i\omega t} \langle \hat{\mu}(0) \cdot \hat{\mu}(t) \rangle_{\text{Kubo}} \\ &\equiv \frac{1}{2\pi} \int_{-\infty}^{\infty} dt e^{-i\omega t} C_{\hat{\mu}\hat{\mu}}^{\text{Kubo}}(t). \end{aligned} \quad (21)$$

Here, $\hat{\mu}$ is the (collective) dipole-derivative operator (the change of the total dipole moment over time). By virtue of Eq. (2), one can also express Eq. (20) in terms of the real part of the standard correlation function

$$\begin{aligned} n(\omega)\alpha(\omega) &= \frac{(1 - e^{-\beta\hbar\omega})}{3cV\varepsilon_0\hbar\omega(1 + e^{-\beta\hbar\omega})} \\ &\times \int_{-\infty}^{\infty} dt e^{-i\omega t} \text{Re}[\langle \hat{\mu}(0) \cdot \hat{\mu}(t) \rangle_{std}]. \end{aligned} \quad (22)$$

Below we show the explicit LSC-IVR (LGA) formulations [Eq. (18)] of the (collective) dipole-derivative correlation functions. By virtue of the relation

$$\hat{A}_{\text{Kubo}}^{\beta} = \frac{i}{\beta\hbar} [\hat{A}, e^{-\beta\hat{H}}], \quad (23)$$

one expands the total dipole moment (which can be a nonlinear function) to the 2nd order

$$\boldsymbol{\mu}(\mathbf{x} + \Delta\mathbf{x}) = \boldsymbol{\mu}(\mathbf{x}) + \frac{\partial\boldsymbol{\mu}}{\partial\mathbf{x}} \cdot \Delta\mathbf{x} + \frac{1}{2} \Delta\mathbf{x}^T \cdot \frac{\partial^2\boldsymbol{\mu}}{\partial\mathbf{x}^2} \cdot \Delta\mathbf{x} + o(\Delta\mathbf{x}^3) \quad (24)$$

and obtains

$$\begin{aligned} f_A(\mathbf{x}_0, \mathbf{p}_0)B(\mathbf{x}_t, \mathbf{p}_t) &\approx \left[\left(\frac{\partial\boldsymbol{\mu}}{\partial\mathbf{x}_0} \right)^T \cdot \mathbf{M}^{-1/2} \mathbf{TQ}^{-1} \cdot \mathbf{P}_0 \right] \cdot \hat{\boldsymbol{\mu}}(\mathbf{x}_t, \mathbf{p}_t) \\ &= \left[\left(\frac{\partial\boldsymbol{\mu}}{\partial\mathbf{x}_0} \right)^T \cdot \mathbf{M}_{\text{therm}}^{-1}(\mathbf{x}_0) \cdot \mathbf{p}_0 \right] \cdot \hat{\boldsymbol{\mu}}(\mathbf{x}_t, \mathbf{p}_t) \end{aligned} \quad (25)$$

for $\langle \hat{\boldsymbol{\mu}}(0) \cdot \hat{\boldsymbol{\mu}}(t) \rangle_{\text{Kubo}}$. Similarly, one has

$$\text{Re} [f_A(\mathbf{x}_0, \mathbf{p}_0)B(\mathbf{x}_t, \mathbf{p}_t)] \approx \hat{\boldsymbol{\mu}}(\mathbf{x}_0, \mathbf{p}_0) \cdot \hat{\boldsymbol{\mu}}(\mathbf{x}_t, \mathbf{p}_t) \quad (26)$$

for the real part of $\langle \hat{\boldsymbol{\mu}}(0) \cdot \hat{\boldsymbol{\mu}}(t) \rangle_{std}$. Note that Eq. (25) has the accuracy to order $o(\Delta\mathbf{x}^3)$ and Eq. (26) to order $o(\Delta\mathbf{x}^2)$, while the dipole or dipole-derivative operator is a nonlinear function of positions and momenta.

We note, in addition to the q-SPC/fw model,¹⁵ the LSC-IVR/classical Wigner model has earlier been applied to a simpler water model for which only single atom velocity correlation functions were calculated.⁴⁶ (The entire imaginary frequency region was not treated consistently though, as discussed in Ref. 7.)

IV. RESULTS AND DISCUSSIONS

A. Simulation details

We first consider two simple point charge models of the 2-atom molecule OH. One is the three-dimensional (3d) shifted Morse potential

$$V(\mathbf{r}) = D_e [1 - \exp[-\alpha(|\mathbf{r}| - r_{eq})]]^2 \quad (27)$$

with the parameters (for the OH stretch⁴⁷) $D_e = 116.09$ kcal/mol, $\alpha = 2.287$ Å⁻¹, and $r_{eq} = 0.9419$ Å. Here, $|\mathbf{r}|$ is the distance between the H-atom and O-atom. The charges on the two atoms are ± 1.1128 e and the masses are $m_H = 1837$ a.u. and $m_O = 16 \times 1823$ a.u. The other is the 3d shifted harmonic potential

$$V(\mathbf{r}) = \frac{1}{2} m_e \omega_e^2 (|\mathbf{r}| - r_{eq})^2. \quad (28)$$

Here, $\omega_e = 3886.56$ cm⁻¹ is the frequency around the minimum of the Morse potential, that is,

$$\frac{1}{2} m_e \omega_e^2 = D_e \alpha^2, \quad (29)$$

with the reduced mass $m_e = m_H m_O / (m_H + m_O)$.

The two 3d models are used to test the accuracy of the LSC-IVR IR vibrational spectrum where exact results are available. Here, we use Eq. (18) [LSC-IVR (LGA)] to calculate the dipole-derivative correlation functions, with $\langle \mathbf{x}_0 | e^{-\beta\hat{H}} | \mathbf{x}_0 \rangle / Z$ in Eq. (18) evaluated by the bisection method⁴⁸ of the path integral Monte Carlo (PIMC). $N_p = 128$ path integral beads are used for $T = 300$ K, while $N_p = 256$ for $T = 100$ K. After the system is equilibrated by PIMC, an initial configuration \mathbf{x}_0 (from a randomly selected path integral bead) is produced every $10N_p$ PIMC steps. The Gaussian distribution for the mass-weighted normal-mode momentum \mathbf{P}_0 in Eq. (14) is used to randomly generate the initial Cartesian momentum $\mathbf{p}_0 = \mathbf{M}^{1/2} \mathbf{TP}_0$ to run a classical trajectory from $(\mathbf{x}_0, \mathbf{p}_0)$ for evaluating the quantities $f_A(\mathbf{x}_0, \mathbf{p}_0)B(\mathbf{x}_t, \mathbf{p}_t)$. The time step of the classical trajectory is ~ 0.05 fs and the velocity Verlet algorithm is used. About 50 000 such classical trajectories are used in order to obtain well-converged results for the correlation functions at long time. (Several hundred trajectories are enough for relatively short time. When using first several periods of the dipole-derivative correlation function to evaluate the peak position of the O–H stretching mode, the time step is decreased to ~ 0.005 fs in order to achieve ~ 1 cm⁻¹ accuracy.) We note that the normal mode frequencies for overall translation and rotation of the complete molecular system are very small ($|\omega_k| \sim 0$) and well separated from the high-frequency vibrational region of interest; one thus simply set the initial normal-mode momenta $\{P_{0,k}\}$ for these normal-modes to zero. Alternatively, one can adopt the procedure in the literature⁴⁹ for the rotational correction.

For the simulation of liquid water, we employ the TTM3-F—the *ab initio* based flexible, polarizable Thole-type model for water clusters and liquid water of Fanourgakis and Xanthreas, which is previously described in Ref. 33. It approximates the dipole moment and the Born-Oppenheimer potential energy surface based on the parameterization which reproduces the binding energies and harmonic vibrational

spectra of small water clusters up to $(\text{H}_2\text{O})_{20}$ given by the second order Møller-Plesset (MP2) electronic structure theory. The TTM3-F model is able to produce good results for static equilibrium structural properties of liquid water with path integral molecular dynamics (PIMD) simulations.^{50–54} More recently, it has been shown that the TTM3-F model reproduces the measured anisotropy and works reasonably well in the librational regime.⁵⁴ One also sees that the dipole-derivative operator is a nonlinear function of the atomic coordinates in the polarizable model.

The LSC-IVR simulation was carried out at $T = 300$ K with the liquid density $\rho_l = 0.997 \text{ g} \times \text{cm}^{-3}$ for a system of 125 water molecules in a box with periodic boundary conditions applied using the minimum image convention. The short-range intermolecular interactions were truncated at an atom-atom distance of $\sim 7.8 \text{ \AA}$, while the long-range electrostatic interactions were treated using Ewald summation. The normal-mode PIMD in the presence of an Andersen thermostat⁵⁵ was performed with $N_p = 32$ beads for the canonical ensemble. The initial position of the classical trajectory was obtained by randomly selecting one of the path integral beads every 1 ps in the imaginary time propagation of the PIMD. About 60 000 such trajectories were used for the correlation functions. (We note that 3000 trajectories are enough to obtain well-converged results for dipole-derivative correlation functions up to 0.1 ps.) Each classical trajectory in the LSC-IVR was propagated up to 2 ps. For the real-time dynamics in the LSC-IVR, the velocity-Verlet algorithm was employed with a time step of $\Delta t = 0.1$ fs. The small time step guarantees the accuracy of the quantity $\dot{\mu}(t)$ by using the finite difference $(\mu(t + \Delta t) - \mu(t - \Delta t))/2\Delta t$ along the real-time trajectory.

Similarly, the classical correlation functions were obtained by propagating 240 classical MD trajectories from independent initial conditions sampled from the classical equilibrium system. Every trajectory was propagated up to 100 ps. Time average was also employed for computing the correlation functions along the MD trajectory.

B. Results and discussions

1. Isolated OH molecule

As pointed out by Liu and Miller in Ref. 15, although the shifted 3d harmonic oscillator (Eq. (28)) is a nonlinear system, it is effectively a linear model when the total angular momentum is set to zero (that is, rotation correction). The LSC-IVR is well known to be exact for fully harmonic potentials. One can also use the classical correlation function as the Kubo-transformed version in Eqs. (20) and (21) to obtain the correct vibrational frequency ω_e for the shifted 3d harmonic oscillator. As shown in Fig. 1, both LSC-IVR and classical MD approaches do not suffer the intrinsic problems (such as the “curvature problem” or “artificial frequencies or resonances”) of other approaches described in Ref. 56.

For real molecular systems, however, the O–H stretch is typically quite anharmonic. For instance, the harmonic approximation (3886.56 cm^{-1}) is significantly blueshifted (by 186 cm^{-1}) from the exact result (3700.55 cm^{-1}) for the char-

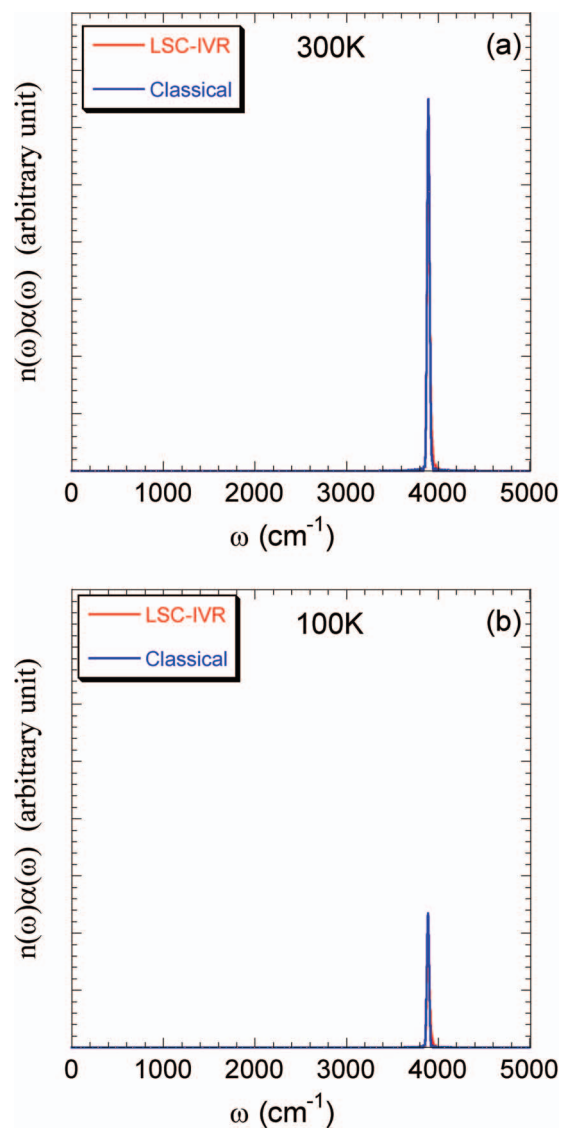


FIG. 1. The IR spectrum of the shifted 3D harmonic potential for the OH molecule. [The same scale for Panels (a) and (b).]

acteristic 3d shifted Morse model (Eq. (27)). Table I and Fig. 2(c) show that the classical results are blueshifted and that they are sensitive to the temperature. The lower the temperature is, the closer to the harmonic approximation and the more blueshifted is the classical result. (Also see, such as, Ref. 49 for *ab initio* MD simulation results.) It is straightforward to understand this well-known blueshift of the classical stretching frequency for the real molecular system: since the classical approach contains no zero-point energy, the system

TABLE I. Peak positions of the O–H stretching mode at different temperatures.

T (K)	$\omega_{\text{OH}} (\text{cm}^{-1})$			
	LSC-IVR	Classical	Exact	Harmonic approx.
300	3782	3864	3700.55	3886.56
200	3783	3871		
100	3783	3878		

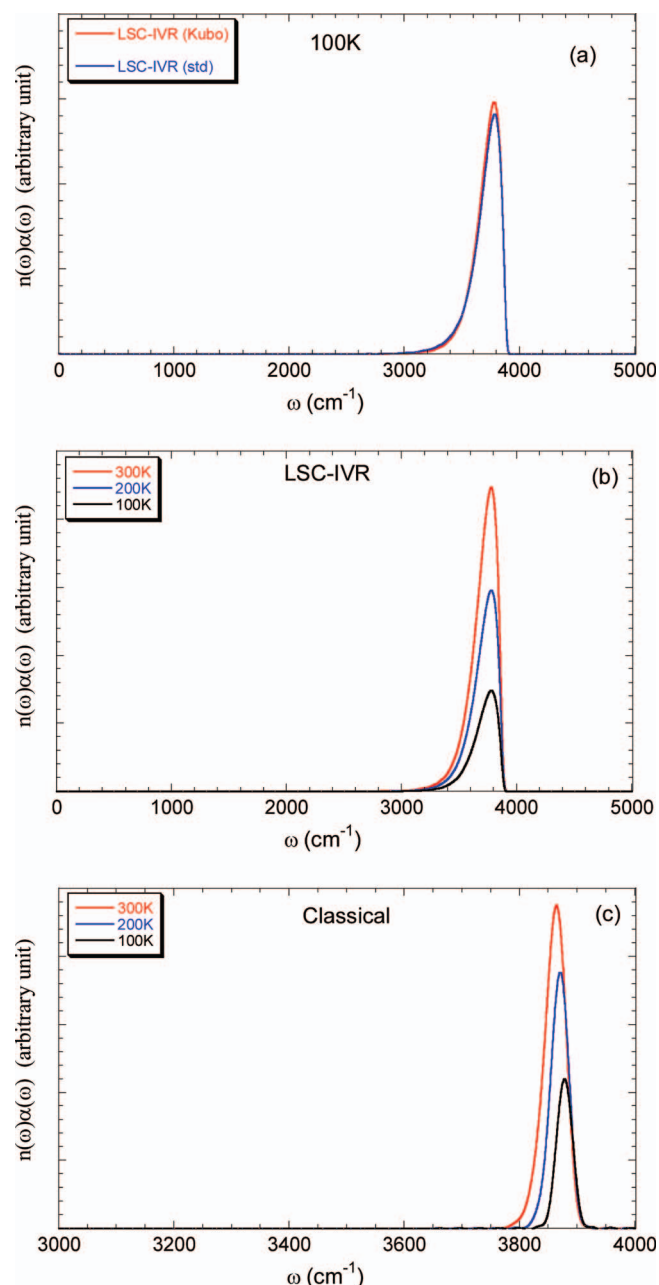


FIG. 2. The IR spectrum of the 3D Morse potential for the OH molecule. (a) Comparison of the LSC-IVR spectrum based on the Kubo-transformed dipole-derivative correlation function to that based on the standard version for $T = 100\text{ K}$. (b) Comparison of the LSC-IVR results at different temperatures. (c) Comparison of the classical results at different temperatures.

oscillates around the harmonic region of the minimum of the well and has little access to the anharmonic region. [A schematic representation is given in Fig. 3(a).] As the temperature increases, the more anharmonic region of the system becomes accessible, but because of the high stretching frequency it is only fully explored at temperature more than $15 \sim 20$ times of room temperature (300 K). In contrast, because the LSC-IVR contains zero-point energy effects, the trajectories are able to access a much wider anharmonic regime [Fig. 3(b)] and thus the LSC-IVR provides a significant improvement over the classical approximation (by as much as 100 cm^{-1}). Table I and Fig. 2(b) show that

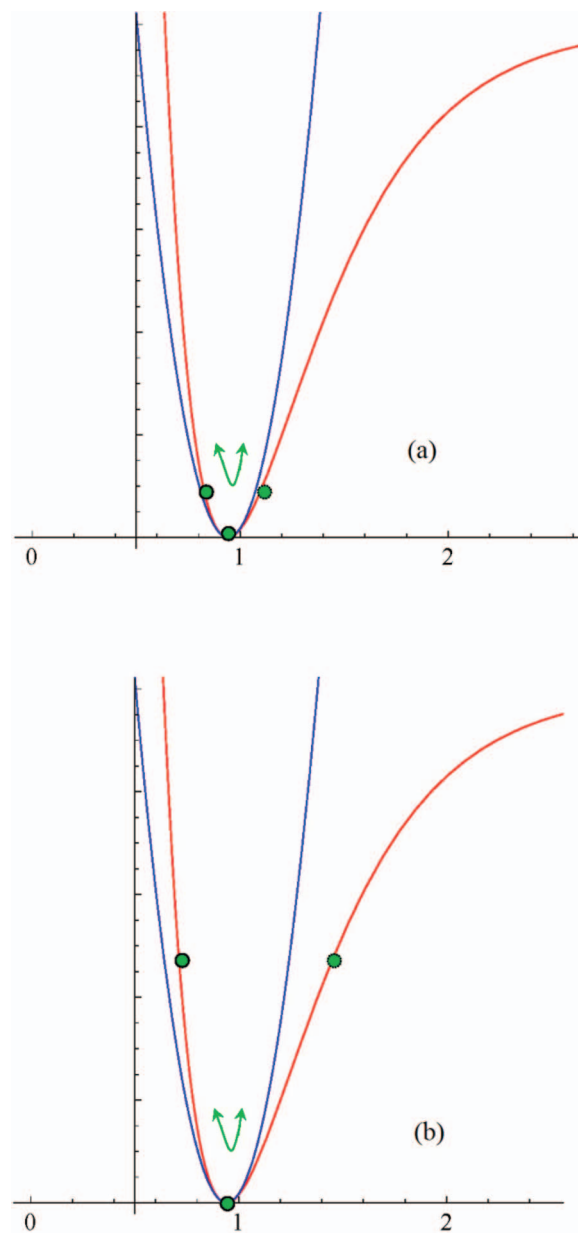


FIG. 3. Schematic representation of the simulation for the Morse potential. Red line illustrates the Morse potential while Blue line shows its harmonic approximation at the minimum of the well. (a) Classical MD trajectories contain no zero-point energy so the regime that the system can reach is controlled by the energy level on the order of $k_B T$. They oscillate around the minimum of the well and predict almost results very close to the harmonic frequency, which are doomed to be blueshifted from the quantum results. (b) Trajectories in the LSC-IVR contain zero-point energy so the region that the system can access is much broader, accounting for the majority of anharmonicity of the potential surface. Because the zero-point energy is much larger than $k_B T$, the LSC-IVR result is insensitive to the change of the temperature.

the LSC-IVR result for the O–H stretch frequency is insensitive to the temperature as the exact result should be, i.e., by virtue of the large amount of the zero-point energy of the high-frequency stretching vibration, the change of temperature has little effects on the LSC-IVR for the isolated OH molecule. That is, the initial phase space distribution in the LSC-IVR varies little as the temperature varies. (For instance, the peak position of the LSC-IVR at 1000 K is $\sim 3783\text{ cm}^{-1}$, same as those for $100\text{--}300\text{ K}$ listed in Table I.) This indicates that the LSC-IVR does not have the intrinsic

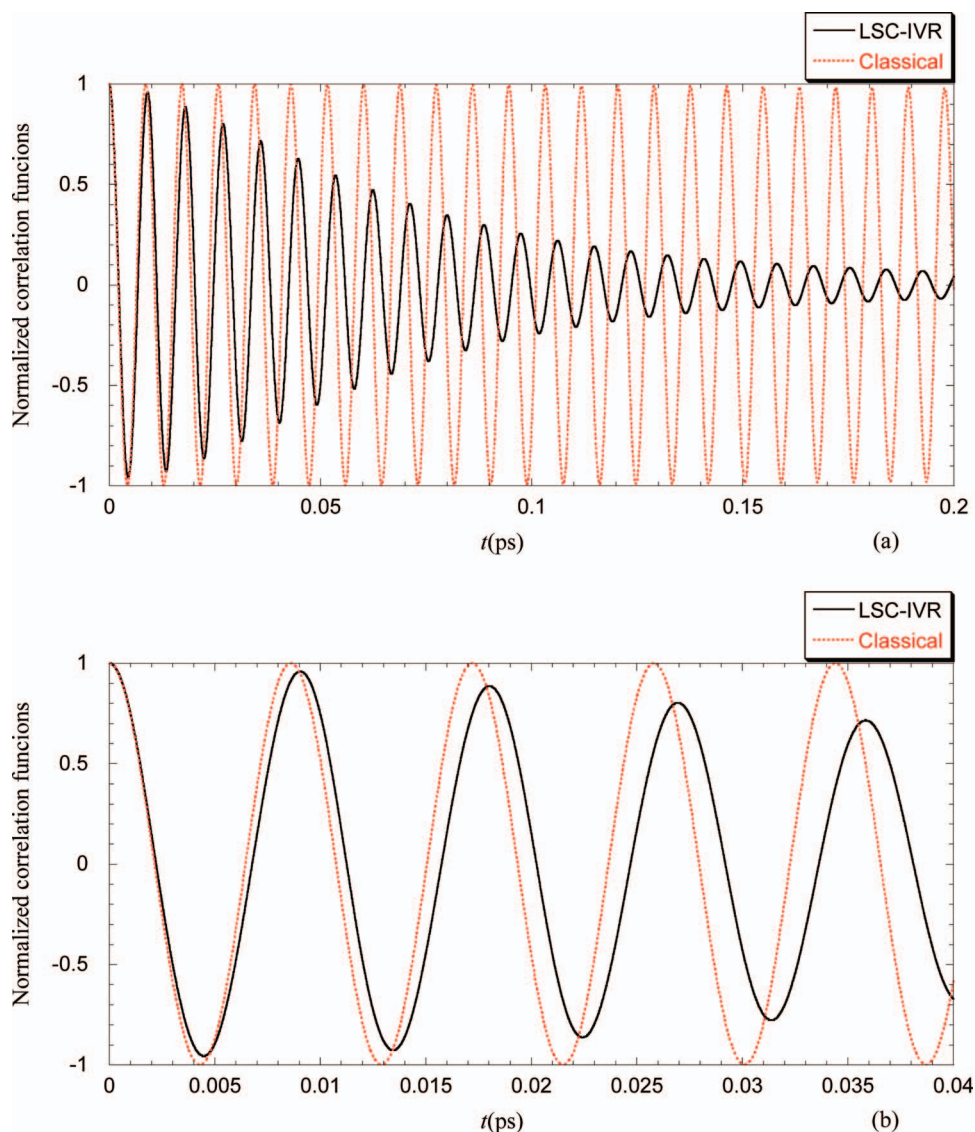


FIG. 4. Normalized dipole-derivative correlation functions $C_{\mu\mu}^{\text{Kubo}}(t)/C_{\mu\mu}^{\text{Kubo}}(0)$ for the 3D Morse potential for $T = 100$ K.

problems of other approaches and does not introduce artificial shifts due to the change of the temperature, which will be very important for the study of the environment effects on the frequency shift in the complex molecular system. [Also see Appendix B.]

However, the LSC-IVR still has a ~ 80 cm^{-1} blueshift from the exact result due to the unphysical decay inherent in the LSC-IVR correlation function for the anharmonic system.^{24–27} (Note both the Kubo-transform and standard versions yield almost the same spectrum as shown in Fig. 2(a).) Apparently, no zero-point energy leakage occurs in the isolated OH molecule, but the LSC-IVR correlation function still demonstrates an unphysical decay that leads a considerable error (~ 80 cm^{-1} blueshift) for the peak position of the O–H stretch. Such an unphysical decay is intrinsic in the LSC-IVR correlation function and leads to the source of error, whether or not so-called zero-point energy leakage exists.

One can improve matters by taking advantage of the fact that the LSC-IVR is a faithful short-time approximation to

quantum dynamics. Thus, if one uses only the first two periods of the LSC-IVR dipole-derivative correlation function [cf. Fig. 4], one obtains almost the exact O–H stretching frequency (3698 cm^{-1}). As seen from Table II, the more periods that one uses, the more blueshifted the result becomes. Alternatively, one can add a damping Gaussian factor in Eqs. (21) or (22) to control the length of time to be used to calculate the spectrum, i.e.,

$$I(\omega) \approx \frac{1}{2\pi} \int_{-\infty}^{\infty} dt e^{-i\omega t} \langle \hat{\mu}(0) \cdot \hat{\mu}(t) \rangle \exp\left[-\frac{t^2}{2\sigma^2}\right]. \quad (30)$$

Here, the width of the Gaussian σ is given by the half time t_{half} based on the relation

$$\exp\left[-\frac{t_{\text{half}}^2}{2\sigma^2}\right] = \frac{1}{2}. \quad (31)$$

TABLE II. Peak positions of the O–H stretching mode estimated by different periods of the LSC-IVR correlation function (same for 100 K and 300 K).

Number of periods	ω_{OH} (cm^{-1})
2	3698
4	3723
6	3739
8	3752
All	3783

(This approach is more useful because it does not require that the time step of the real-time propagation be very small and because one can deal with multi-frequencies.) Using only the short-time part of the correlation function does broaden the peak but gives a much more accurate position of the peak. Table III demonstrates that the shorter the half time t_{half} is employed, the more accurate the result the LSC-IVR yields. One sees that the LSC-IVR can produce nearly exact results ($\pm 5 \text{ cm}^{-1}$) for the high-frequency stretch in either approach by using the correlation function data mainly in first one or two periods. In contrast, classical MD (and other approximate quantum dynamical methods) does not have this merit. We also note the LSC-IVR results in both Tables II and III are insensitive to the change of the temperature for the isolated molecule. One can extend the second approach to study the vibrational IR spectrum for more complex gas phase molecules or clusters (i.e., combined with *ab initio* calculations for the interactions). (One will need to use the parameter t_{half} no shorter than the first period of the bending motion to obtain a good estimate of the peak position of the stretching vibration for the nonlinear molecule.)

We also note that the characteristic 3d shifted Morse potential (Eq. (27)) could be a standard model for investigating accuracy of any other approximate quantum methods.

2. Liquid water

We now focus on the LSC-IVR simulation of the *ab initio* based TTM3-F model for studying quantum dynamical effects in liquid water in ambient condition ($T = 300 \text{ K}$), where the O–H stretch is no longer isolated but interacts with one another in hydrogen-bond networks of the bulk system.

TABLE III. Peak positions of the O–H stretching mode estimated with the Gaussian damping function with different t_{half} parameters (same for 100 K and 300 K).

t_{half} (ps)	ω_{OH} (cm^{-1})
0.010	3705
0.020	3712
0.040	3727
0.060	3739
0.080	3749
0.100	3756
0.120	3761
∞	3783

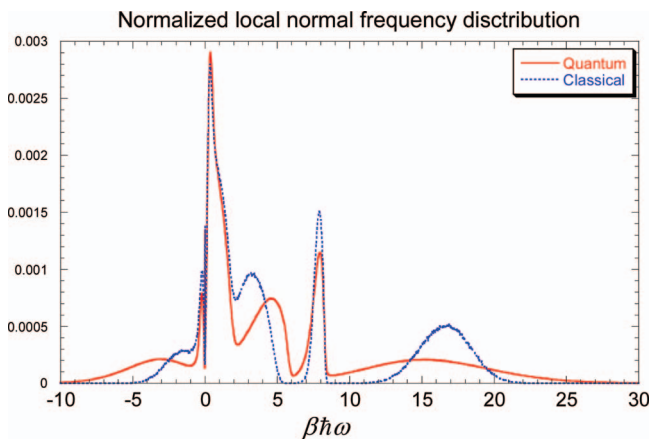


FIG. 5. The normalized local normal frequency distribution of liquid water at $T = 300 \text{ K}$ using the TTM3-F model. (Note $\hbar\beta \sim 208.5 \text{ cm}^{-1}$.)

Figure 5 shows the density distribution of local normal-mode frequencies of typical quantum configurations generated by PIMD for the TTM3-F model at $T = 300 \text{ K}$. One sees that even at room temperature, more than 14% of local frequencies are imaginary, with more than 6% in the “deep tunneling” imaginary frequency regime that have $u_i = \beta\hbar|\omega_i| \geq \pi$. The LGA is able to deal with the entire imaginary frequency regime in the LSC-IVR. The quantum result in Fig. 5 also exhibits that a large amount of high-frequency stretching vibrations in liquid water are more than 15 times of thermal activation energy ($\beta\hbar\omega \geq 15$). As a comparison, Fig. 5 also shows the density distribution of local normal-mode frequencies of typical classical configurations generated by classical MD. Only about 0.7% of classical local frequencies access the “deep tunneling” imaginary frequency regime ($u_i = \beta\hbar|\omega_i| > \pi$). The quantum and classical results are close to each other in the low frequency band arising from the hindered motions ($u \leq 2$ or $\omega \leq 400 \text{ cm}^{-1}$). Significant quantum effects appear again from the high-frequency region for the librational motion to the intermediate regime between the librational and bending bands. This arises from the increase of the frequency of the librational motion caused by the elongation of intramolecular OH bond (in PIMD configurations). The classical density of bending frequencies ($u \sim 8$) is slightly higher than the quantum result. Note that the intensity of the quantum density is much higher than the classical result in the intermediate region between the bending and stretching bands ($u \sim 8.5\text{--}12$), which implies quantum effects exist in this region. One also sees that the quantum density of O–H stretching frequencies is widely spread, while the classical result is much narrower and blueshifted.

Figure 6 shows the comparison of the LSC-IVR dipole-derivative correlation function to the classical one for $T = 300 \text{ K}$. The LSC-IVR and classical results are rather similar, except that the LSC-IVR predicts a more rapid decay of the amplitude and longer oscillation periods of the correlation function than is seen in the classical MD simulation. One also sees that the correlation function in Fig. 6 almost decays to zero within 100 fs. In contrast, the dipole-derivative correlation function of our earlier LSC-IVR application¹⁵ to the q-SPC/fw water model⁵⁷ demonstrates a broad recurrence

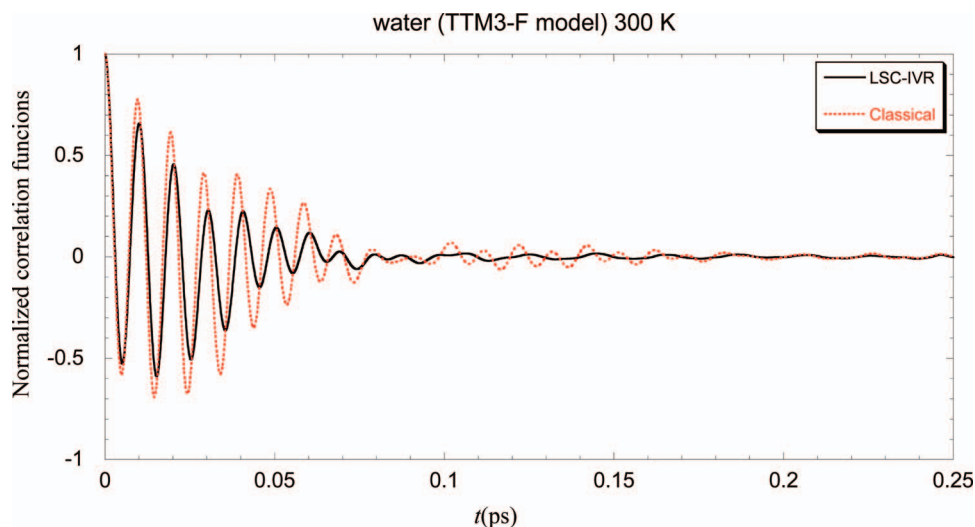


FIG. 6. Normalized dipole-derivative correlation functions $C_{\mu\mu}^{\text{Kubo}}(t)/C_{\mu\mu}^{\text{Kubo}}(0)$ for liquid water at $T = 300$ K using the TTM3-F model.

between 200 and 600 fs, modulated by high-frequency O–H stretching vibrations. This is because that intramolecular O–H stretch is modeled by a 3d shifted harmonic oscillator in the q-SPC/fw model, which gives two distinct peaks for the symmetric and asymmetric O–H stretching modes. Any such recurrence will be absent, yielding a single broad O–H stretching band in the IR absorption spectrum (Fig. 7), while the intramolecular O–H stretch is described by a more realistic anharmonic function in the TTM3-F water model. This is consistent with the simulations of the qTIP4P-F water model in Ref. 30.

Figure 7 shows the simulated IR absorption spectrum in comparison to experiment. We first focus our discussion on the high-frequency O–H stretching band. The classical spectrum (Fig. 7(a)) exhibits a much larger intensity of the O–H stretching band than the experiment data. This is different from the classical result reported in the original paper on the TTM3-F model,³³ because the intensity of the O–H stretching band is sensitive to the time interval of the correlation function data.¹⁵ Our earlier calculation³³ employed an interval that was too large (2.5 fs) in the correlation function to obtain a converged classical IR spectrum. Such a discrepancy in the classical IR spectrum was not pointed out until we carried out the simulations in the present manuscript, albeit the classical results have been shown or compared in places of the literature on the applications of the TTM3-F model.^{52,53,58} Disregarding the intensity of the O–H stretching band, one sees the peak position of the classical result agrees well with experiment (~ 3390 cm^{-1}).

The O–H stretching band produced by the LSC-IVR has a slightly higher intensity compared to experiment. Its peak position (~ 3285 cm^{-1}) is redshifted from the classical result. Although the O–H stretch is in a much more complex environment in liquid water, one expects the anharmonicity of the O–H stretch to remain significant and the conclusion on the isolated O–H molecule to still hold—i.e., the classical O–H stretching band is expected to be blueshifted from the quantum result. Note that the LSC-IVR is most accurate for short time from its original derivations. Vari-

ous applications of the LSC-IVR method have also verified the LSC-IVR correlation function is most reliable for times on the order of the thermal time $\hbar\beta$ for condensed phase systems.^{4,13,14} This implies ~ 25.78 fs at 300 K, which covers the first periods of the bending band. This suggests a value of ~ 3275 cm^{-1} for the peak position of the O–H stretching band of the quantum IR spectrum for the TTM3-F model while using the time scale of the thermal time (25.78 fs) as t_{half} for the damping Gaussian approach [Eq. (30)]. Therefore, one expects classical MD to yield a ~ 115 cm^{-1} blueshift from the suggested quantum result for the peak position of the O–H stretching band for the TTM3-F model, and the LSC-IVR result to yield a blueshift by only ~ 10 cm^{-1} (from the suggested quantum result). It is not surprising to see the blueshift of the LSC-IVR O–H stretching band to be much smaller in liquid water (~ 10 cm^{-1}) than in the isolated (OH) molecular system (~ 80 cm^{-1}). The correlation function inevitably exhibits a physical decay in the condensed phase system due to the quenching effect by coupling among the various degrees of freedom.^{4,37,59,60} The accuracy of the LSC-IVR correlation function thus depends on the competition between the physical decay inherent in the system and the unphysical decay intrinsic in the methodology itself. Once the physical decay dominates, the LSC-IVR produces reliable results.

In contrast, the centroid molecular dynamics (CMD) spectrum⁵³ (Fig. 7(c)) exhibits a slightly larger intensity of the O–H stretching band compared to experiment. Its peak position (~ 3310 cm^{-1}) is also redshifted (by ~ 80 cm^{-1}) from the classical result but blueshifted (by ~ 25 cm^{-1}) from the LSC-IVR result and (by ~ 35 cm^{-1}) from the suggested quantum result. Although the CMD IR spectrum is always redshifted from the exact result for the 3d shifted harmonic oscillator due to the “curvature problem” as pointed out in Ref. 56, it is possible that it can be blueshifted instead for the anharmonic stretching vibrations. In addition to that the quantum result should be blueshifted from the classical and harmonic approximation results as we point out, Fig. 7 (for the TTM3-F model) supports the statement of Ref. 61 that the blueshift due to the “curvature problem” in the CMD high-frequency stretching

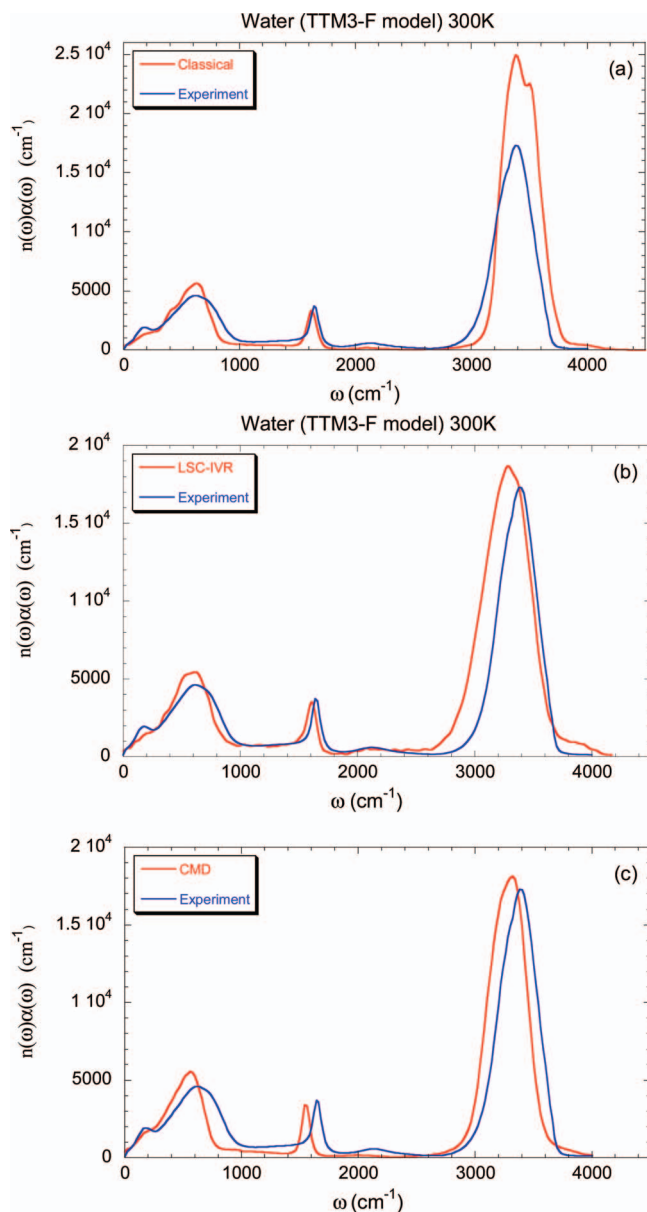


FIG. 7. Comparison of simulated IR spectra using the TTM3-F model to the experimental results.

vibration is much alleviated for liquid water in the ambient condition (~ 300 K). Note that the IR absorption spectrum (same as Fig. 7(c)) given in Ref. 53 is different from that given in Ref. 58. As we have discussed in Ref. 15, different levels of approximation of the CMD model and the time steps involved in updating the CMD trajectory thus affect the high-frequency vibrational band. Although the CMD simulation in Ref. 53 and that in Ref. 58 are all in principle partially adiabatic CMD, the former employs a much smaller time step and sampling time interval (0.02 fs) which likely leads to a better converged CMD IR spectrum. Figure 7 and the above discussion clarify the arguments in the literature^{53,56,58,61} and suggest the quantum result for the peak position of the O–H stretching band for the TTM3-F model.

The intensity and shape of the H–O–H bending band is well reproduced by classical MD for the TTM3-F model (Fig. 7(a)). Its peak position (~ 1620 cm^{-1}) is redshifted by

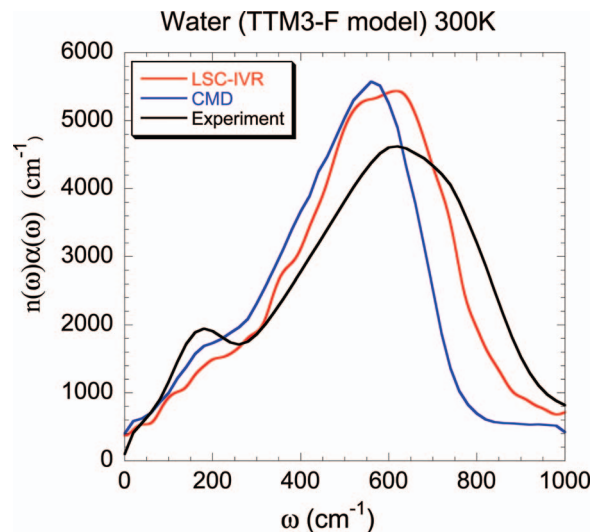


FIG. 8. Comparison of simulated IR spectra in the librational regime.

~ 25 cm^{-1} from experiment (~ 1645 cm^{-1}). One expects the quantum result for the peak position of the bending band for the TTM3-F model to be redshifted as well from the classical result due to anharmonicity. Both the LSC-IVR and CMD yield similarly good results with slightly smaller intensity for the bending band. The peak position is further redshifted from the classical result by ~ 10 cm^{-1} for the LSC-IVR and ~ 75 cm^{-1} for CMD. The LSC-IVR predicts the most satisfactory agreement with experiment for the librational band (below 1000 cm^{-1}), the intermediate region (1000–1500 cm^{-1}) between the librational and bending bands, and that (2000–2200 cm^{-1}) between the bending and stretching bands for the TTM3-F model. For instance, similar to the previous discussion on the density of local frequencies (static property) in Fig. 5, the LSC-IVR IR spectrum (dynamical property) suggests that significant quantum effects exist in this intermediate region (1000–1500 cm^{-1} or $u \approx 4.8$ –7.2) and on the ultrafast energy relaxation from the bending to the libration motion.^{62,63} In contrast, the CMD spectrum (for the TTM3-F model) shows a narrower librational band which indicates the absence of relatively high-frequency hindered rotations (800–1000 cm^{-1}). [See Figs. 7 and 8.] Fig. 7 also shows that both the CMD and classical IR spectra show too lower intensities in the two intermediate regions than experimental results. All simulated (LSC-IVR, classical, and CMD) spectra exhibit the shoulder at ~ 200 cm^{-1} corresponding to the dipole-induced dipole interaction,^{64,65} but the shape is not well reproduced.

Besides the LSC-IVR and CMD, several mixed quantum-classical (QC) approaches^{53,66–68} have been developed for studying the vibrational IR spectrum of such systems as the O–D stretch of HOD in liquid H_2O or the O–H stretch of HOD in liquid D_2O . In such QC approaches, the O–D (O–H) Born-Oppenheimer potential energy curve is obtained by stretching the OD (OH) bond while *fixing* the positions of all other atoms for any configuration (from classical MD or CMD), then the 1d potential surface is used to compute the vibrational frequency and the vibrational stretching band. The mixed QC approaches ignore any response of the surrounding environment due to the change of the selected 1d system

(the chosen O–D or O–H stretch), so the accuracy of the approaches decreases as the coupling between the selected 1d system and its environment becomes stronger.⁵ (One can certainly extend the 1d stretching system to a larger one (e.g., a local monomer⁶⁹) to improve over the mixed QC approaches.) In contrast, the LSC-IVR and CMD treat the whole system on the same footing, so they are more appropriate to study the IR absorption spectrum in *pure* liquid H₂O. [One can compare the LSC-IVR to the mixed QC approaches similar to the recent work⁵³ for studying the vibrational IR spectrum for HOD in H₂O or D₂O with the TTM3-F water model. Further study along these lines would be of interest.]

From the comparison of the spectra in Fig. 7, it is clear that further improvements are needed to the potential of the TTM3-F model³³ in order to achieve a better agreement with experiment (although it has been recently shown the TTM3-F model³³ works well in the librational regime⁵⁴). The good agreement between the peak position of the classical O–H stretching band and experiment actually implies without ambiguity that the TTM3-F model needs to be improved for accurately describing the frequency shifts of hydrogen bonded O–H stretching vibrations, because classical MD fails to account for the significant anharmonicity of the O–H stretching vibration and yields evitable blueshifted frequencies compared to quantum results. As discussed in Refs. 53 and 58, it is possible that the *ab initio* data calculated by the MP2 method for constructing the model were not accurate enough—more advanced electronic structure theory may be necessary. Even if the *ab initio* data were accurate, the parameterization for reproducing the harmonic vibrational spectra of water clusters may also very likely be inadequate, because the anharmonicity might not be well described. Another important factor is that discrepancies inevitably exist between the interactions in small water clusters and those in bulk water. It will be interesting in the future to see how the parameterization of the TTM3-F model changes with more *ab initio* data from larger size water clusters or even systems with periodic boundary conditions. (We note that there exist other *ab initio*-based models^{69–71} for water clusters and liquid water. It might be interesting to apply PIMD and the LSC-IVR/CMD/RPMD to some of these models and compare the simulated properties to those for the TTM3-F model.)

V. CONCLUSION REMARKS

The LSC-IVR is exact in the harmonic limit, regardless of whether the operator is a linear or nonlinear function of positions and momenta and independent of whether it is in the low-frequency regime or involves high-frequency vibrations. The LSC-IVR does not suffer the “curvature problem”⁵⁶ or “artificial frequencies and resonances.”^{56,58,72} It maintains all aspects of the classical coherence and gives correct results for the vibrational IR spectrum of such as the 3d shifted harmonic potential.

However, the LSC-IVR correlation function exhibits intrinsic unphysical decay for the anharmonic molecular system (which also exists in other trajectory-based approximate quantum dynamics methods, see Appendix A). Such unphysical decay in the LSC-IVR correlation function yields an

inevitable blueshift of the high-frequency vibration. For instance, the blueshift is around ~ 80 cm⁻¹ in the present simulations of the 3d shifted Morse oscillator of the isolated OH molecule. Nevertheless, by taking advantage of the short-time data of the LSC-IVR correlation function, one can obtain accurate results for the peak position of the vibrational IR spectrum of the isolated molecule or cluster. The LSC-IVR result (for the peak position of the isolated O–H vibration) is insensitive to the change of the temperature as the exact value should be. This suggests that the LSC-IVR could be a reliable method to study the temperature dependence for more complex systems.

Because the inherent physical decay of the condensed phase system compensates the intrinsic unphysical decay of the LSC-IVR methodology, the blueshift problem in the anharmonic vibration is much alleviated in the large molecular system. One expects ~ 10 cm⁻¹ for the blueshift of the LSC-IVR O–H stretching band for the TTM3-F model for liquid water at 300 K from the quantum result. The stronger the couplings are, the more dominate the physical decay is and the more accurate the LSC-IVR is, which is entirely consistent with the previous investigation on a conventional condensed phase model (i.e., a simple system coupled with the harmonic oscillators environment).⁷³ The investigation of the present manuscript supports the arguments in Refs. 15 and 30 that the LSC-IVR is a good approximate quantum approach for study of the IR absorption spectrum.

Comparison of the simulated IR spectra for the TTM3-F water model shows that the intensity of the O–H stretching band given by classical MD is much higher than that by the LSC-IVR or CMD. The peak position of the O–H stretching band given by CMD is blueshifted from that by the LSC-IVR, and the H–O–H bending band given by CMD is redshifted from the LSC-IVR result. While the CMD librational band indicates the absence of relatively high-frequency hindered rotations (800–1000 cm⁻¹) for the TTM3-F water model, the LSC-IVR result implies that such motions still exist in liquid water for the same model that agrees well with experiment. In agreement with experiment and similar to the discussion on the static density distribution of local frequencies (Fig. 5), the LSC-IVR IR spectrum suggests significant quantum effects in the intermediate region (1000–1500 cm⁻¹) between the bending and librational bands and that (2000–2200 cm⁻¹) between the stretching and bending bands.

Liu and Miller have recently proposed several approaches^{24–27,74} which conserve the canonical distribution in the phase space formulation of quantum mechanics and improve over the LSC-IVR on the intrinsic unphysical decay for the long-time behaviors. Such approaches in the Wigner phase space representation reduce to the LSC-IVR in the harmonic limit, so it is trivial to show that they give the correct result for such as the isolated 3d harmonic vibrational oscillator. It will be interesting to apply them to the *ab initio*-based models for studying quantum dynamical effects for water clusters and liquid water. (Also see Appendix A for more discussion.)

Finally, we note that cautions need to be taken for using the condensed phase model—a simple system coupled with a harmonic bath environment⁷⁵ (system+harmonic bath), while

degrees of freedom for high-frequency stretching modes are involved. As shown in the current simulations, the classical MD result of O–H stretching band has a large blueshift (~ 150 – 200 cm^{-1}) because it fails to account for the large anharmonicity for obtaining the correct frequencies. The conventional approach—employing the spectrum computed by classical MD to obtain the harmonic bath variables for the environment—will not be reasonable when such as O–H stretches in the hydrogen bond network of liquid water play an important role.

ACKNOWLEDGMENTS

This work was supported by the National Science Foundation Grant No. CHE-0809073 and by the Director, Office of Science, Office of Basic Energy Sciences, Chemical Sciences, Geosciences, and Biosciences Division, U.S. Department of Energy under Contract No. DE-AC02-05CH11231. We acknowledge a generous allocation of supercomputing time from the National Energy Research Scientific Computing Center (NERSC) and the use of the Lawrence computational cluster resource provided by the IT Division at the Lawrence Berkeley National Laboratory. J.L. acknowledges the 2011 NERSC initiative for scientific exploration award. G.S.F. acknowledges a grant provided by the E. U. Seventh Framework Program FP7/2007-2013 (Grant No. 205066). S.S.X. acknowledges the support by the Chemical Sciences, Geosciences, and Biosciences Division, Office of Basic Energy Sciences, U.S. Department of Energy at Pacific Northwest National Laboratory. Battelle operates the Pacific Northwest National Laboratory for the U.S. Department of Energy. S.S. acknowledges Grant-in-Aid for Scientific Research (Grant No. 22350013) and Grant-in-Aid for Challenging Exploratory Research (Grant No. 23655020) supported by Japan Society for the Promotion of Science. We also thank Francesco Paesani for providing the CMD results.

APPENDIX A: DISCUSSION ON ZERO-POINT ENERGY EFFECTS AND VARIOUS TRAJECTORY-BASED APPROXIMATE QUANTUM DYNAMICS METHODS

Classical dynamics conserves the value of the classical time-independent Hamiltonian $H(x, p)$. Given that initial conditions are from the equilibrium distribution (such as the canonical distribution $e^{-\beta H(x, p)}$), classical dynamics also conserves the distribution. For example, a classical MD trajectory simultaneously conserves the energy and the distribution when the canonical ensemble approaches the microcanonical ensemble $\delta(E - \hat{H})$ in the thermodynamic limit (i.e., the number of particles $N \rightarrow \infty$ and the volume of the system $V \rightarrow \infty$) for the ergodic system. Apparently, any fictitious dynamics that conserves the equilibrium distribution but fails to do so for the energy will cause artificial effects as long as real-time dynamics is of concern.⁷⁷

Quantum dynamics simultaneously preserves the values both of the Hamiltonian \hat{H} and of the Boltzmann operator $e^{-\beta \hat{H}}$. Any trajectory-based approximate quantum dynamics method that has been applied to condensed phase systems, however, conserves only one property in the mapping

phase space. The approaches based on conservation of different properties are often not identical, except for the harmonic system where quantum coherences reduce to classical coherences. For instance, when the Wigner phase space representation of quantum mechanics is chosen, conservation of the mapping Hamiltonian for energy (which is equivalent to the classical Hamiltonian) yields the LSC-IVR/classical Wigner model, while conservation of the mapping canonical distribution function generates the three families of trajectory-based dynamics as proposed in the literature.^{24–27} As Liu and Miller analyze in a forthcoming paper,⁷⁴ the former conservation leads to more accurate short-time dynamics, while the latter favors long-time dynamical behaviors.

PIMD conserves the mapping canonical distribution in the extended phase space.^{78,79} For instance, one mapping option is $e^{-\beta H_n/N_P}$ with

$$H_n = \sum_{j=1}^{N_P} \left[\frac{p_j^2}{2m} + \frac{1}{2} m \omega_P^2 (x_j - x_{j+1})^2 + V(x_j) \right] \quad (32)$$

subject to the cyclic boundary condition $x_{N_P+1} = x_1$, where N_P is the number of path integral beads and $\omega_P = N_P/\hbar\beta$. The dynamics generated by the fictitious Hamiltonian Eq. (32) yields an isomorphism to the thermodynamics in the canonical ensemble of quantum mechanics. RPMD by Manolopoulos *et al.* employs an *ad hoc* assumption that the fictitious dynamics [generated by Eq. (32)] in PIMD can be useful for obtaining the real-time dynamics information.^{30,32,58,80–83} Apparently, the mapping canonical distribution is preserved with the dynamics in RPMD. However, RPMD (and CMD) is incapable to give exact nonlinear correlation functions even for a one-dimensional harmonic potential.^{7,12,13,24,26,84} Due to “artificial frequencies or resonances,”^{56,58,72} RPMD even fails to generate the correct *linear* correlation function for the shifted 3d harmonic oscillator⁵⁶ (Eq. (28)) which is effectively a linear model under rotation correction.¹⁵ [As a comparison, the LSC-IVR gives correct results for these systems.] More discussion on RPMD, CMD, and the LSC-IVR and its improved versions can be found in the literature.^{7,12,13,24,26,30,56,85} Following the discussion in the previous paragraph, it is not subtle at all for one to see that RPMD does not conserve the *true* mapping Hamiltonian for energy in the extended phase space, which is

$$\tilde{H}_E = \frac{1}{N_P} \sum_{j=1}^{N_P} \left[\frac{p_j^2}{2m} - \frac{1}{2} m \omega_P^2 (x_j - x_{j+1})^2 + V(x_j) \right]. \quad (33)$$

Subtle is how the failure of conservation of Eq. (33) along the RPMD trajectory causes unphysical influences to the short- and long-time behaviors of the RPMD model for the real-time correlation function. Similar to the LSC-IVR that preserves the mapping Hamiltonian for energy, one can construct a model [i.e., ring polymer Hamiltonian dynamics (RPHD)] for computing the real-time correlation function by employing the dynamics generated by Eq. (33). RPHD will give exact results in the classical and high temperature limits and also for the correlation function involving linear functions of position or momentum in the harmonic limit for

one-dimensional systems, same as RPMD does. “Artificial frequencies or resonances”^{56,58,72} in the high (real) frequency regime might be much alleviated in RPHD because the artificial frequencies arising from the beads are imaginary instead. On the other hand, as RPHD does not necessarily preserve the mapping canonical distribution, it has the same drawback as that of the LSC-IVR. It will be interesting to test such a RPHD model and compare it with RPMD for some condensed phase systems. Similarly, it is straightforward to extend the above discussion to CMD. For example, CMD conserves the mapping canonical distribution but fails to conserve the mapping Hamiltonian for energy.

We note that cautions should be taken while discussing zero-point energy effects in liquid water. It is of no doubt that energy exchange between the intramolecular and intermolecular modes occurs in real-time dynamics of liquid water. While the zero-point energy of the intramolecular modes and that of the intermolecular modes should be preserved on ensemble average, the total (zero point) energy of the system has to be “microscopically” conserved. As mentioned in Ref. 15 and as discussed in more details in Ref. 30, the LSC-IVR fails for the former and leads to the artificial energy flow from the intramolecular modes to the intermolecular ones (i.e., zero-point energy leakage). [Apparently, the zero-point energy leakage is a part of the effects caused by the failure of the LSC-IVR—the mapping canonical distribution is not conserved.] It will be interesting to investigate its effects on the intrinsic unphysical decay of the LSC-IVR correlation function in liquid water. On the other hand, in addition to the nonlinear operator problem^{7,12,13,19,24,26,30,84–86} and the “curvature problem”⁵⁶ or “artificial frequencies or resonances,”^{56,58,72} CMD/RPMD fails in “microscopically” preserving the true energy estimator along its trajectories and cannot give a faithful description on the zero-point energy effects in liquid water either (although CMD/RPMD can give the correct ensemble average value for the energy estimator because the mapping canonical distribution is conserved). It will also be of future interests to quantify how this affects the simulation results for liquid water.

In summary, no current trajectory-based approximate quantum dynamics methods exist to describe zero-point energy effects (and/or quantum decoherence) without any ambiguity. [Ref. 87 suggests that zero-point energy effects could actually involve quantum interference.] The challenging question now is, whether it is possible to construct a kind of phase space to generate trajectory-based dynamics that conserve both the mapping Hamiltonian for energy and the mapping canonical distribution?

APPENDIX B: ANOTHER POSSIBLE MICROSCOPIC ORIGIN FOR ACCURACY OF THE LSC-IVR RESULT FOR THE HIGH-FREQUENCY ANHARMONIC STRETCH

With $\hbar = 1$, the eigen-energy level of the Morse potential Eq. (27) is

$$E(n) = \left(n + \frac{1}{2}\right) \omega_e - \left(n + \frac{1}{2}\right)^2 \frac{\omega_e^2}{4D_e}. \quad (34)$$

The quantum transition frequency ω_{01} between the ground and first excited state becomes

$$E(1) - E(0) = \omega_e - 2\frac{\omega_e^2}{4D_e}. \quad (35)$$

The classical frequency with action-angle variables for the Morse potential⁷⁶ is

$$E'(n) = \omega_e - \frac{\omega_e^2}{4D_e}(2n + 1). \quad (36)$$

Note that $E'(1/2) = \omega_e - 2(\omega_e^2/4D_e)$ is equal to the quantum transition frequency. That is, when a classical trajectory is propagated at the average of the initial and final action variables [an energy about half-way between the “ground” and “first excited” state $E'(0)$ and $E'(1)$], the classical frequency matches the quantum transition frequency!

The linearized approximation in the LSC-IVR (Ref. 5) makes the “sum and difference” transformation of the classical variables, so that the classical mechanics is run at the average of the initial and final variables. Although this is done for convenience in Cartesian coordinates rather than action-angle variables, it is roughly equivalent.

- ¹W. H. Miller, *Adv. Chem. Phys.* **25**, 69 (1974).
- ²W. H. Miller, *Adv. Chem. Phys.* **30**, 77 (1975).
- ³W. H. Miller, *Proc. Natl. Acad. Sci. U.S.A.* **102**(19), 6660 (2005).
- ⁴W. H. Miller, *J. Chem. Phys.* **125**(13), 132305 (2006).
- ⁵H. Wang, X. Sun, and W. H. Miller, *J. Chem. Phys.* **108**(23), 9726 (1998).
- ⁶Q. Shi and E. Geva, *J. Chem. Phys.* **118**(18), 8173 (2003).
- ⁷J. Liu and W. H. Miller, *J. Chem. Phys.* **131**, 074113 (2009).
- ⁸X. Sun, H. Wang, and W. H. Miller, *J. Chem. Phys.* **109**(17), 7064 (1998).
- ⁹T. Yamamoto, H. B. Wang, and W. H. Miller, *J. Chem. Phys.* **116**(17), 7335 (2002).
- ¹⁰J. Liu, B. J. Alder, and W. H. Miller, *J. Chem. Phys.* **135**, 114105 (2011).
- ¹¹J. Liu and W. H. Miller, *J. Chem. Phys.* **125**(22), 224104 (2006).
- ¹²J. Liu and W. H. Miller, *J. Chem. Phys.* **127**, 114506 (2007).
- ¹³J. Liu and W. H. Miller, *J. Chem. Phys.* **128**(14), 144511 (2008).
- ¹⁴J. Liu and W. H. Miller, *J. Chem. Phys.* **129**(12), 124111 (2008).
- ¹⁵J. Liu, W. H. Miller, F. Paesani, W. Zhang, and D. Case, *J. Chem. Phys.* **131**, 164509 (2009).
- ¹⁶Q. Shi and E. Geva, *J. Phys. Chem. A* **107**, 9059 (2003).
- ¹⁷Q. Shi and E. Geva, *J. Phys. Chem. A* **107**, 9070 (2003).
- ¹⁸B. J. Ka and E. Geva, *J. Phys. Chem. A* **110**(31), 9555 (2006).
- ¹⁹Q. Shi and E. Geva, *J. Chem. Phys.* **119**(17), 9030 (2003).
- ²⁰J. A. Poulsen, G. Nyman, and P. J. Rossky, *J. Chem. Theory Comput.* **2**(6), 1482 (2006).
- ²¹J. A. Poulsen, G. Nyman, and P. J. Rossky, *J. Chem. Phys.* **119**(23), 12179 (2003).
- ²²T. Yamamoto and W. H. Miller, *J. Chem. Phys.* **118**(5), 2135 (2003).
- ²³E. Pollak and J. S. Shao, *J. Chem. Phys.* **116**(4), 1748 (2002).
- ²⁴J. Liu and W. H. Miller, *J. Chem. Phys.* **126**, 234110 (2007).
- ²⁵J. Liu and W. H. Miller, *J. Chem. Phys.* **134**, 104101 (2011).
- ²⁶J. Liu and W. H. Miller, *J. Chem. Phys.* **134**, 104102 (2011).
- ²⁷J. Liu, *J. Chem. Phys.* **134**, 194110 (2011).
- ²⁸J. Liu, A. Nakayama, and N. Makri, *Mol. Phys.* **104**(8), 1267 (2006).
- ²⁹G. A. Voth and T. D. Hone, *J. Chem. Phys.* **122**(5), 057102 (2005).
- ³⁰S. Habershon and D. E. Manolopoulos, *J. Chem. Phys.* **131**(24), 244518 (2009).
- ³¹P. L. McRobbie and E. Geva, *J. Phys. Chem. A* **113**(39), 10425 (2009).
- ³²B. J. Braams and D. E. Manolopoulos, *J. Chem. Phys.* **125**(12), 124105 (2006).
- ³³G. S. Fanourgakis and S. S. Xantheas, *J. Chem. Phys.* **128**(7), 074506 (2008).
- ³⁴B. J. Berne and G. D. Harp, *Adv. Chem. Phys.* **17**, 63 (1970).
- ³⁵W. H. Miller, S. D. Schwartz, and J. W. Tromp, *J. Chem. Phys.* **79**(10), 4889 (1983).
- ³⁶R. Kubo, M. Toda, and N. Hashitsume, *Statistical Physics II: Nonequilibrium Statistical Mechanics*, 2nd ed. (Springer-Verlag, Heidelberg, 1991).

- ³⁷W. H. Miller, *J. Phys. Chem. A* **105**(13), 2942 (2001).
- ³⁸R. Hernandez and G. A. Voth, *Chem. Phys.* **233**(2–3), 243 (1998).
- ³⁹E. P. Wigner, *Phys. Rev.* **40**, 749 (1932).
- ⁴⁰E. Wigner, *Phys. Rev.* **40**(5), 749 (1932).
- ⁴¹E. J. Wigner, *Trans. Faraday Soc.* **34**, 29 (1938).
- ⁴²E. J. Heller, *J. Chem. Phys.* **65**, 1289 (1976).
- ⁴³H. W. Lee and M. O. Scully, *J. Chem. Phys.* **73**(5), 2238 (1980).
- ⁴⁴E. Pollak and J. L. Liao, *J. Chem. Phys.* **108**(7), 2733 (1998).
- ⁴⁵We note that a typo exists in Eq. (2.6) of Ref. 15. That is, $\beta\hbar$ was missing in the right term of Eq. (2.6). The correct equation [Eq. (20)] was in fact used in Ref. 15 though.
- ⁴⁶J. A. Poulsen, G. Nyman, and P. J. Rossky, *Proc. Natl. Acad. Sci. U.S.A.* **102**(19), 6709 (2005).
- ⁴⁷S. Habershon, T. E. Markland, and D. E. Manolopoulos, *J. Chem. Phys.* **131**(2), 024501 (2009).
- ⁴⁸D. M. Ceperley, *Rev. Mod. Phys.* **67**, 279 (1995).
- ⁴⁹P. Kumar and D. Marx, *Phys. Chem. Chem. Phys.* **8**(5), 573 (2005).
- ⁵⁰G. S. Fanourgakis, G. K. Schenter, and S. S. Xantheas, *J. Chem. Phys.* **125**(14), 141102 (2006).
- ⁵¹F. Paesani, S. Luchi, and G. A. Voth, *J. Chem. Phys.* **127**, 074506 (2007).
- ⁵²F. Paesani and G. A. Voth, *J. Phys. Chem. B* **113**(17), 5702 (2009).
- ⁵³F. Paesani, S. S. Xantheas, and G. A. Voth, *J. Phys. Chem. B* **113**, 13118 (2009).
- ⁵⁴F. Paesani, S. Yoo, H. J. Bakker, and S. S. Xantheas, *J. Phys. Chem. Lett.* **1**(15), 2316 (2010).
- ⁵⁵H. C. Andersen, *J. Chem. Phys.* **72**(4), 2384 (1980).
- ⁵⁶A. Witt, S. D. Ivanov, M. Shiga, H. Forbert, and D. Marx, *J. Chem. Phys.* **130**(19), 194510 (2009).
- ⁵⁷F. Paesani, W. Zhang, D. A. Case, T. E. Cheatham, and G. A. Voth, *J. Chem. Phys.* **125**(18), 184507 (2006).
- ⁵⁸S. Habershon, G. S. Fanourgakis, and D. E. Manolopoulos, *J. Chem. Phys.* **129**(7), 074501 (2008).
- ⁵⁹N. Makri and K. Thompson, *Chem. Phys. Lett.* **291**, 101 (1998).
- ⁶⁰K. Thompson and N. Makri, *J. Chem. Phys.* **110**, 1343 (1999).
- ⁶¹F. Paesani and G. A. Voth, *J. Chem. Phys.* **132**(1), 014105 (2010).
- ⁶²S. Ashihara, N. Huse, A. Espagne, E. T. J. Nibbering, and T. Elsaesser, *J. Phys. Chem. A* **111**(5), 743 (2007).
- ⁶³S. Ashihara, S. Fujioka, and K. Shibuya, *Chem. Phys. Lett.* **502**(1–3), 57 (2011).
- ⁶⁴B. Guillot, *J. Chem. Phys.* **95**(3), 1543 (1991).
- ⁶⁵M. Sharma, R. Resta, and R. Car, *Phys. Rev. Lett.* **95**(18), 187401 (2005).
- ⁶⁶S. Mukamel, *Principles of Nonlinear Optical Spectroscopy* (Oxford University Press, New York, 1995).
- ⁶⁷H. J. Bakker and J. L. Skinner, *Chem. Rev.* **110**(3), 1498 (2010).
- ⁶⁸E. Harder, J. D. Eaves, A. Tokmakoff, and B. J. Berne, *Proc. Natl. Acad. Sci. U.S.A.* **102**(33), 11611 (2005).
- ⁶⁹Y. Wang and J. M. Bowman, *J. Chem. Phys.* **134**(15), 154510 (2011).
- ⁷⁰R. Kumar, F.-F. Wang, G. R. Jenness, and K. D. Jordan, *J. Chem. Phys.* **132**(1), 014309 (2010).
- ⁷¹Y. Wang, X. Huang, B. C. Shepler, B. J. Braams, and J. M. Bowman, *J. Chem. Phys.* **134**(9), 094509 (2011).
- ⁷²M. Shiga and A. Nakayama, *Chem. Phys. Lett.* **451**(4–6), 175 (2008).
- ⁷³H. Wang, M. Thoss, K. L. Sorge, R. Gelabert, X. Gimenez, and W. H. Miller, *J. Chem. Phys.* **114**, 2562 (2001).
- ⁷⁴J. Liu and W. H. Miller, “A note on the short-time and long-time behaviors of trajectory-based approximate quantum dynamics methods” (unpublished).
- ⁷⁵A. J. Leggett, S. Chakravarty, A. T. Dorsey, M. P. A. Fisher, A. Garg, and M. Zwenger, *Rev. Mod. Phys.* **59**, 1 (1987).
- ⁷⁶Here, we consider the classical case. We note that the Semiclassical Wentzel-Kramers-Brillouin (WKB) approximation is able to reproduce exact energy levels for the Morse potential.
- ⁷⁷D. Frenkel and B. Smit, *Understanding Molecular Simulation: From Algorithms to Applications* (Academic, Saint Diego, 2002).
- ⁷⁸D. Chandler and P. G. Wolynes, *J. Chem. Phys.* **74**, 4078 (1981).
- ⁷⁹M. Parrinello and A. Rahman, *J. Chem. Phys.* **80**, 860 (1984).
- ⁸⁰I. R. Craig and D. E. Manolopoulos, *J. Chem. Phys.* **121**(8), 3368 (2004).
- ⁸¹I. R. Craig and D. E. Manolopoulos, *J. Chem. Phys.* **122**(8), 084106 (2005).
- ⁸²T. F. Miller and D. E. Manolopoulos, *J. Chem. Phys.* **122**(18), 184503 (2005).
- ⁸³T. F. Miller and D. E. Manolopoulos, *J. Chem. Phys.* **123**(15), 154504 (2005).
- ⁸⁴A. Horikoshi and K. Kinugawa, *J. Chem. Phys.* **122**(17), 174104 (2005).
- ⁸⁵I. R. Craig and D. E. Manolopoulos, *Chem. Phys.* **322**(1–2), 236 (2006).
- ⁸⁶T. D. Hone and G. A. Voth, *J. Chem. Phys.* **121**(13), 6412 (2004).
- ⁸⁷W. H. Miller, *J. Phys. Chem. A* **113**(8), 1405 (2009).